Materials and Design 37 (2012) 268–273

Contents lists available at SciVerse ScienceDirect

Materials and Design

journal homepage: www.elsevier.com/locate/matdes

In situ synthesis of TiN/Ti_3Al intermetallic matrix composite coatings on Ti6Al4V alloy

Z.D. Liu, X.C. Zhang *, F.Z. Xuan, Z.D. Wang, S.T. Tu

Key Laboratory of Pressurized System and Safety, MOE School of Mechanical Engineering, East China University of Science and Technology, Shanghai 200237, PR China

ARTICLE INFO

Article history:
Received 2 November 2011
Accepted 6 December 2011
Available online 14 December 2011

Keywords:
A. Intermetallics
F. Microstructure
A. Composite coating

ABSTRACT

The aim of this paper was to develop an in situ method to synthesize the TiN reinforced Ti_3Al intermetallic matrix composite (IMC) coatings on Ti6Al4V alloy. The method was divided into two steps, namely depositing pure Al coating on Ti6Al4V substrate by using plasma spraying, and laser nitriding of Al coating in nitrogen atmosphere. The microstructure and mechanical properties of TiN/Ti_3Al IMC coatings synthesized at different laser scanning speeds (LSSs) in laser nitriding were investigated. Results showed that the crack- and pore-free IMC coatings can be made through the proposed method. However, the morphologies of TiN dendrites and mechanical properties of coatings were strongly dependent on LSS used in nitriding. With decreasing the LSS, the amount and density of TiN phase in the coating increased, leading to the increment of microhardness and elastic modulus and the decrement of fracture toughness of coating. When the LSS was extremely high (i.e., 600 mm/min), only a thin TiN/Ti_3Al layer with thickness around of 100 μm was formed near the coating surface.

1. Introduction

Titanium and its alloy are widely used in aerospace applications owing to their excellent corrosion resistance, strength-to-weight ratio, and high-temperature strength [1]. A more specific non-aerospace application of titanium alloy is the use as low-pressure (LP) steam turbine blades in ultra-supercritical and nuclear power plants. The high strength-to-weight ratio of titanium alloys allows them to replace chromium steels in LP blades requiring high strength and fracture toughness. The turbine efficiency can be improved by maximizing the conversion from steam to energy through lengthening the final row of blades [2]. However, to satisfy the rapidly increasing energy requirement, the turbines need to operate at high temperatures and speeds, leading to high possibility of failure. Liquid impact erosion is one of the main major causes of turbine blade failure. Protecting the blade surface with erosion resistant coating is one of the feasible solutions to overcome this superficial damage results from liquid impact [3].

A common technique used to improve the wear and corrosion resistance of titanium alloys is to nitride the surface [4]. Different methods have been developed for this purpose, such as solid-state nitriding by chemical vapor deposition and molten-state nitriding by laser. Among these methods, laser nitriding have received wide attention in recent years since it offered several advantages such as a high nitrogen concentration, accurate position control, and without any undesired heating effect on substrate through the reaction between a laser molten top layer and nitrogen [5]. Up to present, a number of researches have been carried out to investigate the microstructure, mechanical properties, corrosion and wear resistance of the laser nitrided titanium alloy [6–10]. However, it should be noted that the major concern for laser nitriding of titanium alloys was to avoid cracking. The roughness and hardness of the surface layer could cause a concentration of tensile stress, which led to perpendicular cracking when the critical stress value was exceeded during the cooling process [11].

Different methods have been developed to prevent the formation of cracks in laser nitriding process. These methods can be divided into three approaches. In the first approach, the cracks can be avoided through adjusting the processing parameters in laser nitriding. Xue et al. used invemulti-variable test method to optimize the parameters for the laser gas nitriding process to avoid surface cracking [12]. Previous researches showed that preheating the substrate to reduce the cooling rate [13] or diluting the nitrogen environment [14] can reduce the tendency of cracking. However, the preheating treatment may lead to the decrement of the hardness of nitrided coating [15]. The second approach was developed on the basis of the concept of stress assisted diffusion. Xuan et al. [16] investigated the laser surface nitriding of Ti6Al4V alloy under external stresses. It was interesting to find that the defect-free nitrided coating could be achieved using a millisecond Nd:YAG laser coupled with an optimum applied stress. However, the

* Corresponding author at: Key Laboratory of Pressurized System and Safety, Ministry of Education, Meilong Road 130, Xuhui District, Shanghai 200237, PR China. Tel.: +86 21 64253149; fax: +86 21 64250328.
E-mail address: xczhang@ecust.edu.cn (X.C. Zhang).

0261-3069/$ - see front matter © 2011 Elsevier Ltd. All rights reserved.
doi:10.1016/j.matdes.2011.12.008

magnitude of the optimum stress cannot be easily selected since it was related to the laser parameters such as laser power and scanning speed. The third approach, in which the cracking can be prevented through adding some chemical elements such as nickel and chromium in the coating, was developed by Fu and Batchelor [17]. Although the wear resistance of the nitride coating may increase due to the formation of the Cr_2N phases, the corrosion resistance of the coating cannot be ensured. Researches by Hirose et al. [18] and Guo et al. [19] showed that Ti_3Al intermetallic coating synthesized on pure Ti by laser alloying can significantly increase the corrosion and oxidation resistance of substrate.

The aim of this paper was to develop a novel method through which the TiN reinforced Ti_3Al intermetallic matrix composite (IMC) coatings can be in situ synthesized. The method can be divided into two steps, namely depositing pure Al coating on Ti6Al4V substrate by using plasma spraying, and laser nitriding of Al coating in nitrogen atmosphere. The effect of laser scanning speed (LSS) in laser nitriding on the microstructure and mechanical properties of TiN/Ti_3Al IMC coatings was also investigated.

2. Experimental details

2.1. Material

The Ti6Al4V alloy with basketweave microstructure, produced by Shanghai research institute of nonferrous metals, China, was used for laser nitriding in this paper. This alloy had a nominal chemical composition of (by wt.%) 5.7 Al, 4.1 V, 0.05 Fe, 0.08 C, 0.13 O, 0.03 N and balance Ti. Fig. 1 showed the cross-sectional microstructure of Ti–6Al–4V alloy. The yielding and the ultimate tensile strengths of the alloy were respectively 864 MPa and 978 MPa, and the elastic modulus was 113 GPa. The specimens were cut in the form of plates ($22 \times 10 \times 5$ mm) by using wire electrical discharge cutting machine. The coating was prepared at the middle of 22×10 mm surface. Before plasma spraying and laser nitriding, the specimen surface was grinded with 600 grit SiC papers, and then cleaned ultrasonically with acetone.

2.2. Coating preparation

The TiN/Ti_3Al IMC coating was fabricated through a two-step method. In the first step, the pure Al coating was deposited onto the Ti6Al4V alloy plate by using conventional air plasma spraying system developed by Beijing aeronautical manufacturing technology research institute, China. The pure Al powder with the purity higher than 99% fabricated by Beijing general research institute of mining and metallurgy, China, was used as the coating material. The powder was characterized by near-perfect spherical particles with the diameter in the range of 50–100 μm. Prior to spraying, the substrates were cleaned in acetone solution and preheated to 100–200 °C, and then sandblasted using the corundum powder. For sandblasting and spraying, the substrates were fixed by the corresponding fixtures. The parameters used for plasma spraying were listed in Table 1. The primary gas used in the plasma spraying was argon, with hydrogen as secondary gas. The spray distance was kept to be 150 mm. For all coated specimens, the coating thicknesses were controlled to be around 150 μm.

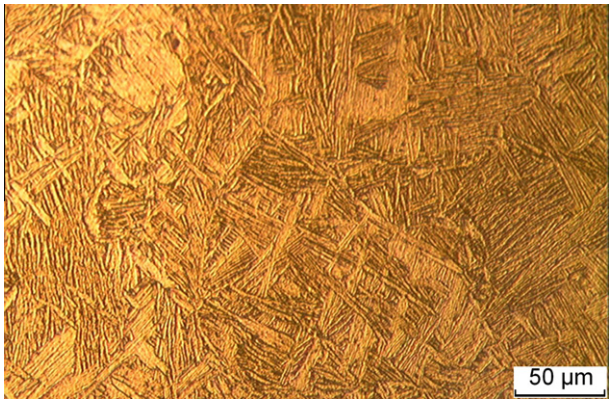

Fig. 1. Cross-sectional microstructure of Ti–6Al–4V alloy.

Table 1
Details of plasma spraying parameters.

Argon gas flow rate (L/min)	Hydrogen gas flow rate (L/min)	Voltage (V)	Current (A)	Powder feed rate (g/min)
40	10	60	600	30

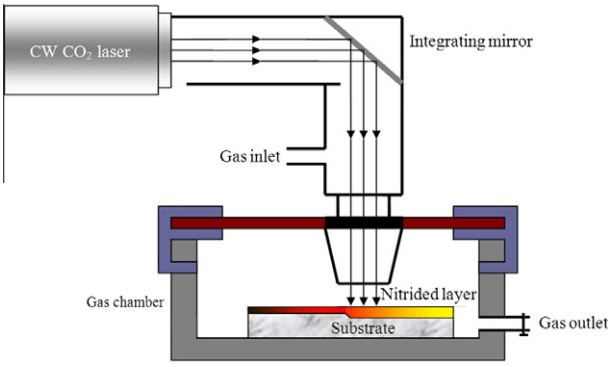

Fig. 2. Schematic showing the nitriding experimental set-up.

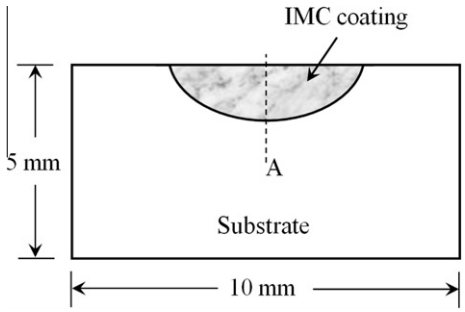

Fig. 3. Schematic showing the measured location of microhardness and elastic modulus in the coating.

In the second step, the laser nitriding of Al coated specimen was carried out in nitrogen atmosphere. Since the elements Ti and Al were prone to be oxidized, the laser nitriding was carried out in a nitrogen-filled chamber to prevent oxidation. Prior to laser nitriding, the nitrogen was bubbled into the chamber continuously for 5 min. The experimental set-up of a laser gas nitriding process was illustrated schematically in Fig. 2. A coaxial nozzle containing shielding gas channel was used to supply the nitrogen atmosphere. The laser used in this investigation was a 5-kW CO_2 laser operating in a continuous mode. The laser processing was conducted on a material processing system equipped with a four-axis computer numerical controlled (CNC) laser material processing machine tool. The laser beam was focused by an integral lens with a focal length of 200 mm. The diameter of the focused laser beam was around 6.0 mm. Five levels of laser scanning speeds (LSS), namely 200, 300, 400, 500, 600 mm/min, were used to investigate the effect of nitrogen LSS on the properties of coatings. Other processing

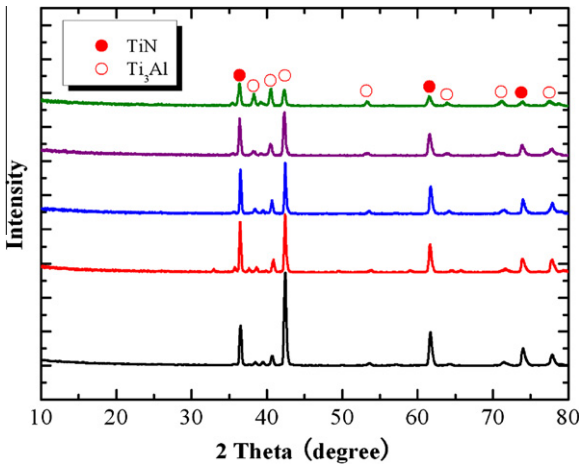

Fig. 4. XRD patterns of the TiN/Ti_3Al IMC coatings.

parameters used for laser nitriding were listed as follows: nitrogen gas flow rate 100 l/min, output power of laser beam 2.7 kW.

2.3. Characterization of coating

The microstructures and morphologies of coatings were observed by using a ZEISS EVO® MA 15 scanning electron microscope (SEM). Prior to observations, the coated specimens were mounted in the epoxy resin. The cross-sectional surface for SEM observation was wet-ground with 400, 600, 800 and 1200 grit SiC paper. The specimens were ultrasonically cleaned in water and then in acetone between each grit paper. The polished specimen etched in a solution of HF, HNO_3 and H_2O with a volume ratio of 5:5:90 at room temperature for approximately 10 s before the SEM investigation. The phases in the TiN/Ti_3Al IMC coatings were identified by means of X-ray diffraction (XRD) with Cu Kα (l = 1.54 Å) radiation, step 0.02° on a D8-Advance apparatus.

The microhardness profiles along the depth direction near the center of the TiN/Ti_3Al IMC coatings were determined by a MH-5 Vickers microhardness tester at 0.5 N with a dwell time of 5 s. The elastic modulus profiles along the depth direction of the coatings were measured by using the Knoop indentation technique with the indentation load of 500 g and dwell time of 15 s. The location in the coating for microhardness and elastic modulus measurement is schematically denoted as route A in Fig. 3. The theoretical background on determining elastic modulus of a material using the Knoop indentation testing was given by Marshall et al. [20] and Leigh et al. [21]. The elastic modulus of coating can be evaluated by

$$14299\frac{\alpha P}{Ea}@b - b^{\epsilon} \quad (1)$$

where E is the elastic modulus, P is the indenter load in N, α is a constant, 0.45, a and b are the major and minor diagonals of the ideal Knoop indentation; $b/a = 0.14$, b^{e} is the minor diagonal of the measured Knoop indentation. For a given distance to the coating surface, eight indentations were randomly produced to get representative values of elastic modulus. Indentions were spaced

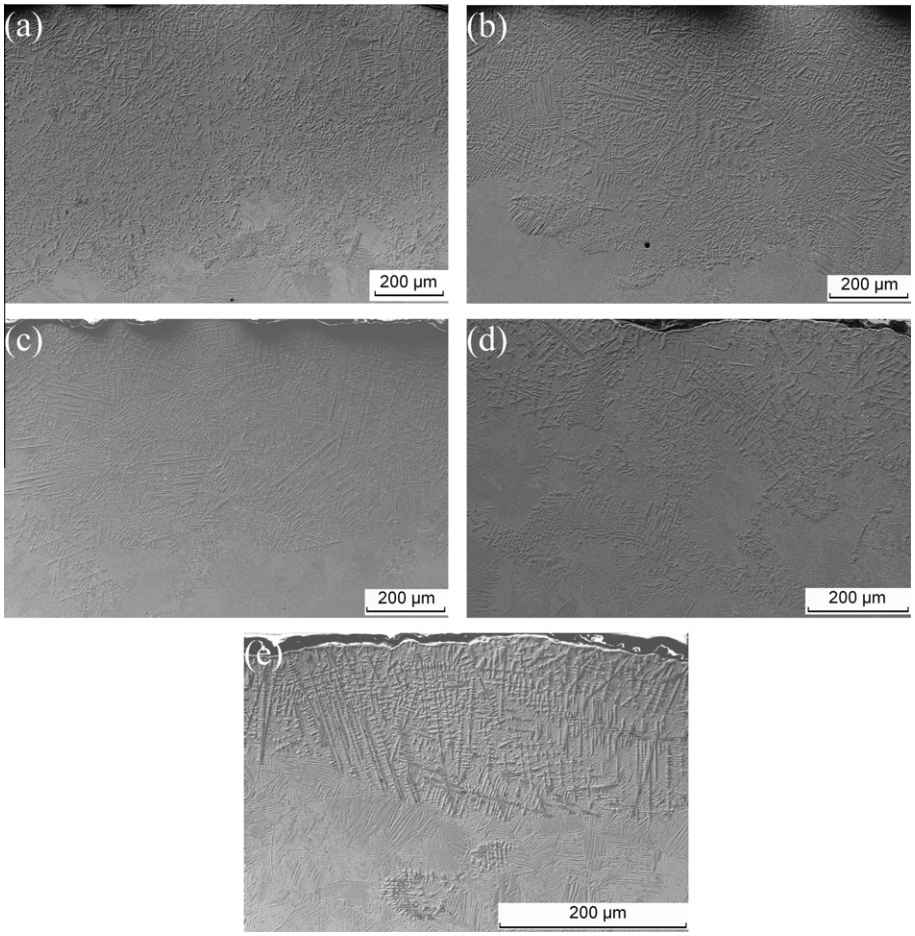

Fig. 5. Overview microstructure on the cross section of the TiN/Ti_3Al IMC coatings synthesized at laser scanning speed of (a) 200 mm/min, (b) 300 mm/min, (c) 400 mm/min, (d) 500 mm/min, and (e) 600 mm/min.

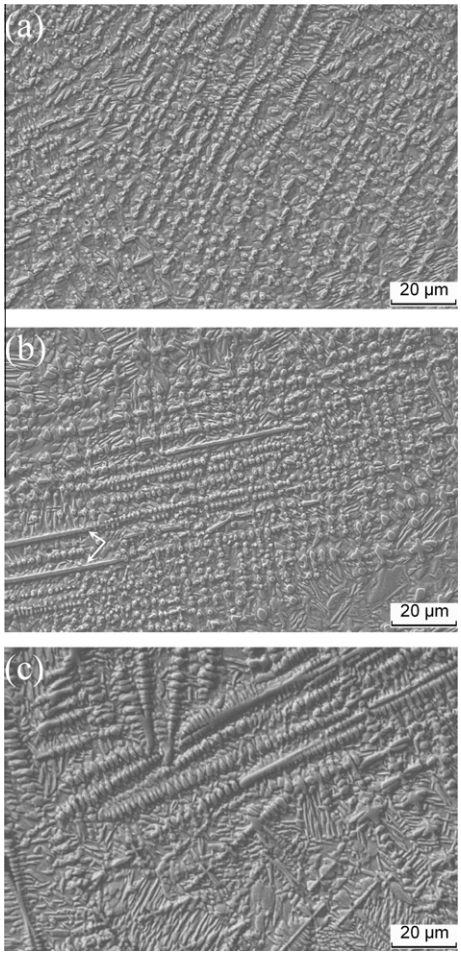

Fig. 6. SEM micrographs of the TiN/Ti_3Al IMC coatings synthesized at different laser scanning speeds in the middle zone, (a) 200 mm/min, (b) 400 mm/min, and (c) 600 mm/min.

sufficiently far apart so that the indention behavior was not affected by the adjacent indentations. The fracture toughness of the coating was evaluated by using Vickers indentation. Five indentations were randomly produced to get representative values of fracture toughness. A Vickers load was applied on a polished cross-section of the coating and the crack lengths induced by the indentation were subsequently measured. The following formula was utilized for the determination of the fracture toughness,

$$K_{Ic} = 0.016\left(\frac{E}{H}\right)^{1/2}\frac{P}{c^{3/2}} \quad (2)$$

where c is the crack length in coating measured from the center of the indent.

3. Results and discussion

3.1. Microstructure

The X-ray diffraction patterns of the coatings synthesized at different LSSs are shown in Fig. 4. It can be revealed that the crystalline phases of TiN/Ti_3Al IMC coating consist mainly of Ti_3Al intermetallic phase and TiN reinforced phase. The peaks located at about 36.2 corresponding to TiN is observed in all coatings. The relative intensity of TiN peaks decreases with increasing LSS when the LSS is higher than 400 mm/min. The similar results were also obtained by Yu et al. [22]. Generally, at high LSS, the interaction time between the laser beam and the elements Ti and Al will be low. The amount of the TiN should be low in such a case. When the LSS is extremely high, the temperature and its gradient in the coating during laser nitriding may be not changed obviously by increasing the scanning speed. In such a case, the amount of TiN may be not strongly depended on the LSS.

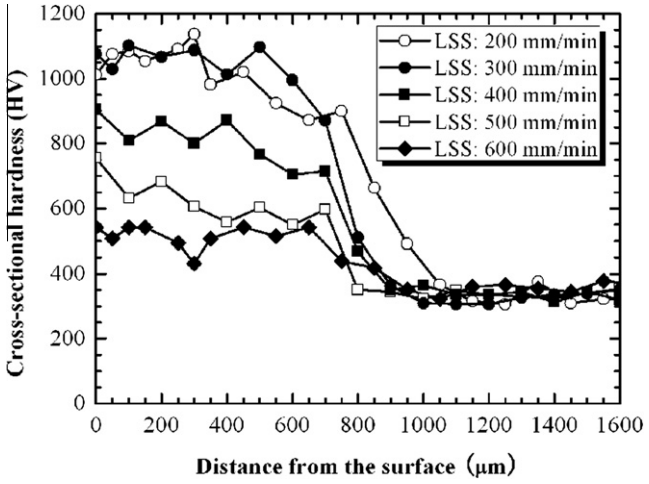

Fig. 7. Through-thickness microhardness profile in the TiN/Ti_3Al IMC coatings synthesized at different laser scanning speed.

The overview microstructures on the cross section of the TiN/Ti_3Al IMC coatings synthesized at five different LSSs are shown in Fig. 5. It can be seen that all TiN/Ti_3Al IMC coatings were metallurgically bonded to the substrate. No cracks or pores can be found in the coatings. When the LSS is lower than 400 mm/min, the volume fraction of the needle-like and granular-like TiN dendrites embedded in the Ti_3Al intermetallic matrix is high. The TiN phase is distributed homogeneously in the coating. The maximum depths of the IMC coatings are higher than 600 μm. When the LSS is 500 mm/min, only a small amount of TiN phase can be found in the layer with a thickness around of 200 μm near the surface of coating. Moreover, the distribution of the TiN phase is sparse in some areas. When the LSS is extremely high, i.e., 600 mm/min, the TiN phase only exists near the surface of coating. These results are in accordance with the XRD results in Fig. 3.

Fig. 6a–c shows the microstructures in the middle zones of the TiN/Ti_3Al IMC coatings fabricated at different LSSs. When the LSS is 200 mm/min, the TiN phase with granular-like morphology is embedded in the Ti_3Al intermetallic matrix. When the LSS is 400 mm/min, some undeveloped TiN phase can be found, as indicated by the arrows in Fig. 5b. When the LSS is 60 mm/min, the TiN dendrites become coarser and some needle-like dendrites can be found. When the Al coating was irradiated by high-energy laser beam in nitrogen atmosphere, melting of the Ti and Al occur to form the liquid Ti(Al) solid solution immediately at the high temperature according to Ti–Al binary phase diagram presented by Murray [23]. Finally, a Ti_3Al coating was formed during the subsequent rapid cooling process. Simultaneously, there was an exothermic reaction between nitrogen and the liquid Ti(Al) solid solution due to the great affinity of Ti for nitrogen, from which the TiN phase was produced [24]. Thus, a TiN reinforced Ti_3Al matrix composite coating was obtained. In addition, under low LSS, there will be more TiN phase formed in the liquid Ti(Al) solid solution due to the sufficient reaction of Ti and N.

3.2. Micro-hardness and elastic modulus

Fig. 7 shows the microhardness profile along the depth direction of the TiN/Ti_3Al IMC coatings. By comparing with the Ti6Al4V

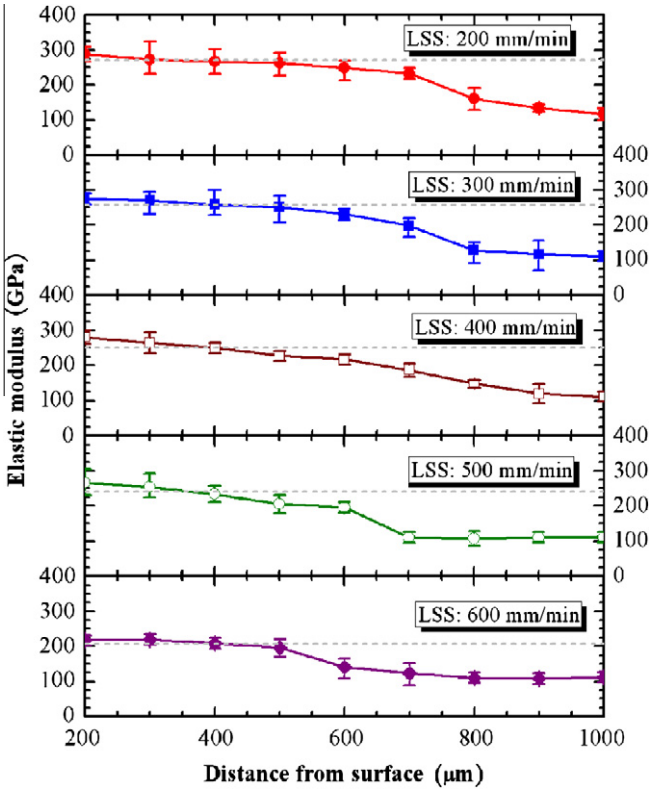

Fig. 8. Through-thickness elastic modulus profile in the TiN/Ti_3Al IMC coatings synthesized at different laser scanning speed.

alloy substrate, the TiN/Ti_3Al IMC coatings exhibit higher microhardness. The hardness distribution within the coatings is wavy. In the coating/substrate bonding zone, the microhardness decreases gradually to the substrate. Generally, with increasing the LSS, the microhardness in the coating decreases. This phenomenon is expected, since the amount of TiN phase in the coating decreases with increasing the LSS, as seen in Figs. 5 and 6. It is well known that an addition of hard phase in a soft matrix can increase the hardness of a material [19]. Thus, the microhardness of the TiN/Ti_3Al IMC coatings was much higher than that of Ti_3Al, and it increased with the increasing TiN volume fraction. For the coating synthesized at LSS lower than 400 mm/min, the cross-sectional hardness of TiN/Ti_3Al IMC coatings varied drastically with the depth of the coating, which may be attributed to the inhomogeneous distribution of the hard TiN phase.

Fig. 8 shows the elastic modulus profiles along the depth direction of the TiN/Ti_3Al IMC coatings, where the dash lines indicate the average elastic modulus of coating. It can be found that the fluctuation of the measured elastic moduli in the coating through the depth direction is small for the given coatings. The average elastic modulus of coating generally decreases with increasing the LSS, as seen in Fig. 9. When the LSS is extremely high, i.e., 600 mm/min, the elastic modulus of coating is around 208 GPa, which is slightly higher than the elastic modulus of Ti_3Al intermetallic compound and film [25,26].

3.3. Fracture toughness

The measured fracture toughness of the TiN/Ti_3Al IMC coatings synthesized at different LSSs is shown in Fig. 10. The effect of LSS on the fracture toughness is clear. With increasing the LSS, the fracture toughness of coating decreases. The phenomenon is due to the amount TiN reinforced phase decreases with increasing the LSS. The measured values of fracture toughness of the coatings are in

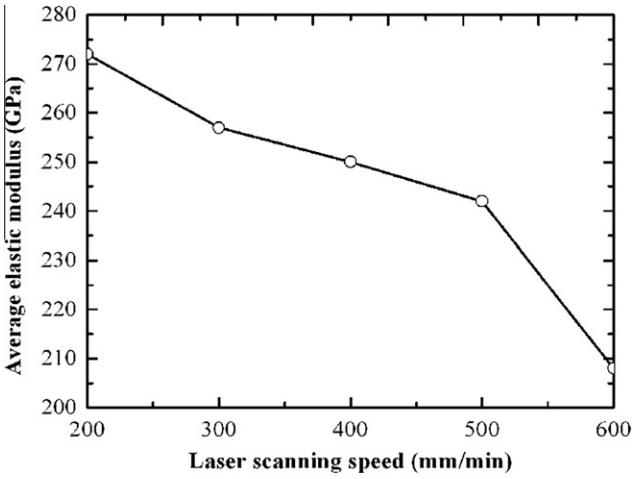

Fig. 9. Effect of laser scanning speed on the average elastic modulus of TiN/Ti_3Al IMC coatings.

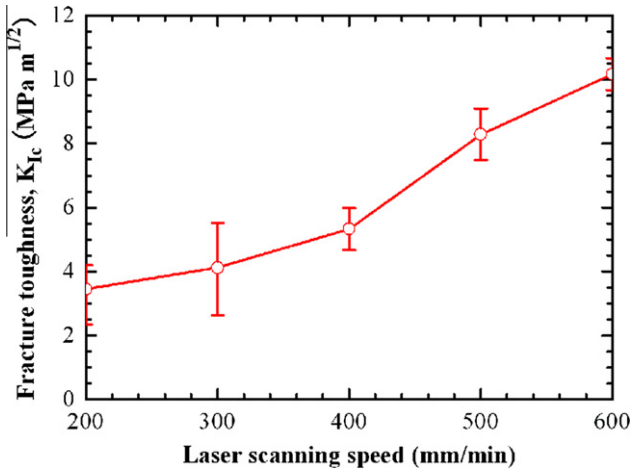

Fig. 10. Variation of fracture toughness of TiN/Ti_3Al IMC coating along with laser scanning speed.

the range of 2.34–10.67 MPa $m^{1/2}$. The reported fracture toughness of bulk TiN and TiN films ranges from 2.0 MPa $m^{1/2}$ to 8.0 MPa $m^{1/2}$ [27,28]. For the TiN/Ti_3Al IMC coatings synthesized at LSS lower than 500 mm/min, the measured data of fracture toughness agree well with the previously experimental results. For the coating synthesized at LSS of 600 mm/min, the measured fracture toughness of the coating is around 10.17 MPa $m^{1/2}$, which is lower than the fracture toughness of Ti_3Al coatings reported by Guo et al. [29]. For the Ti_3Al coatings fabricated by laser cladding on pure Ti substrate, the measured fracture toughness by Guo et al. was in the range of 11.7–72.3 MPa $m^{1/2}$, which was dependent on the Al amount in coatings.

4. Conclusions

A novel method was developed to synthesize the TiN reinforced Ti_3Al intermetallic matrix composite (IMC) coatings on Ti6Al4V alloy in the present paper. The method was divided into two steps, namely depositing pure Al coating on Ti6Al4V substrate by using plasma spraying, and laser nitriding of Al coating in nitrogen atmosphere. It was found that the microstructure and mechanical properties of IMC coating was strongly depended on the processing parameters, such as laser scanning speed. Generally, with increasing the laser canning speed, the volume fraction of TiN reinforced

phase in the coating decreased, leading to the decrement of microhardness and elastic modulus and the increment of fracture toughness of the coating. Moreover, The TiN phase exhibited granular-like at low laser canning speed. At high laser canning speed, the TiN phase showed needle-like morphology.

Acknowledgements

The authors are grateful for the support by National Natural Science Foundations of China (50805047, 51175177) and National High-tech R&D Program of China (863 Program, 2009AA044803). The author X.C. Zhang is also grateful for the support by Ph.D. Programs Foundation of Ministry of Education of China (20090101120021).

References

[1] Noda T. Application of cast gamma TiAl for automobiles. Intermetallics 1998;6:709–13.
[2] Mann BS, Arya V, Pant BK. Influence of laser power on the hardening of Ti6Al4V low-pressure steam turbine blade material for enhancing water droplet erosion resistance. J Mater Eng Perform 2011;20:213–8.
[3] Duraiselvam M, Galun R, Siegmann S, Wesling V, Mordike BL. Study of liquid impact erosion in B2-NiTi and Ti_3Al based intermetallic matrix composites on laser alloyed Ti–6Al–4V. Adv Eng Mater 2007;9:171–6.
[4] Jacobs MH. Surface engineering of materials. Mater Design 1993;14:33–7.
[5] Schaaf P. Laser nitriding of metals. Prog Mater Sci 2002;47:1–161.
[6] Yilbas BS, Nickel J, Coban A, Sami M, Shuja SZ, Aleem A. Laser melting of plasma nitride Ti-6A1–4V alloy. Wear 1997;212:140–9.
[7] Xin H, Watson LM, Baker TN. Surface analytical studies of a Laser nitrided Ti–6Al–4V alloy: a comparison of spinning and stationary laser beam modes. Acta Mater 1998;46:1949–61.
[8] Naeem M, Preston ME, Tyrer JR. Processing of engineering ceramics with high power CO_2 lasers. Mater Design 1989;10:281–5.
[9] Abboud JH, Fidel AF, Benyounis KY. Surface nitriding of Ti–6Al–4V alloy with a high power CO_2 laser. Opt Laser Technol 2008;40:405–14.
[10] Razavi RS, Salehi M, Ramazani M, Man HC. Corrosion behaviour of laser gas nitride Ti–6Al–4V in HCl solution. Corros Sci 2009;51:2324–9.
[11] Fu Y, Wei J, Batchelor AW. Some considerations on the mitigation of fretting damage by the application of surface modification technologies. J Mater Process Technol 2000;99:231–45.
[12] Xue L, Islam M, Koul AK, Bibby M, Wallace W. Laser gas nitriding of Ti–6Al–4V part 1: optimization of the process. Adv Perform Mater 1997;4:25–47.
[13] Hu C, Baker TN. The importance of preheat before laser nitriding a Ti–6Al–4V alloy. Mater Sci Eng 1999;A265:268–75.
[14] Pérez MG, Harlan NR, Zapirain F, Zubiri F. Laser nitriding of an intermetallic TiAl alloy with a diode laser. Surf Coat Technol 2006;200:5152–9.
[15] Raaif M, El-Hossary FM, Negm NZ, Khalil SM, Kolitsch A, Höche D, et al. CO_2 laser nitriding of titanium. J Phys D: Appl Phys 2008;41:085208-1–8-8.
[16] Xuan FZ, Cao LQ, Wang ZD, Tu ST. Laser surface nitriding of Ti6Al4V alloy coupled with an external stress field. J Mater Res 2010;25:344–9.
[17] Fu YQ, Batchelor AW. Laser nitriding of pure titanium with Ni, Cr for improved wear performance. Wear 1998;214:83–90.
[18] Hirose A, Ueda T, Kobayashi KF. Wear and oxidation properties of titanium aluminides formed on titanium surface by laser alloying. Mater Sci Eng 1993;A160:143–53.
[19] Guo BG, Zhou JS, Zhang ST, Zhou HD, Pu YP, Chen JM. Microstructure and tribological properties of in situ synthesized TiN/Ti_3Al intermetallic matrix composite coatings on titanium by laser cladding and laser nitriding. Mater Sci Eng 2008;A480:404–10.
[20] Marshall DB, Noma T, Evans AG. A simple method for determining elastic-modulus-to-hardness ratios using knoop indentation technique. J Am Ceram Soc 1982;65:c175–6.
[21] Leigh SH, Lin CK, Berndt CC. Elastic response of thermal spray deposits under indentation tests. J Am Ceram Soc 1997;80:2093–9.
[22] Yu HJ, Sun FJ, Zhang J. Laser and plasma nitriding of titanium using CW-CO_2 laser in the atmosphere. Curr Appl Phys 2009; 1009; 9: 227–33.
[23] Murray JL. Phase diagrams of binary titanium Alloys, ASM International, Metals Park, OH; 1987.
[24] Nwobu AIP, Rawlings RD, West DRF. Nitride formation in titanium based substrates during laser surface melting in nitrogen-argon atmospheres. Acta Mater 1999;47:631–43.
[25] Liu YL, Liu LM, Wang SQ, Ye HQ. First-principles study of shear deformation in TiAl and Ti_3Al. Intermetallics 2007;15:428–35.
[26] Chinmulgund M, Inturi RB, Barnard JA. Effect of Ar gas pressure on growth, structure, and mechanical properties of sputtered Ti, Al, TiAl, and Ti_3Al films. Thin Solid Films 1995;270:260–3.
[27] Moriyama M, Aoki H, Kobayashi Y, Kamata K. The mechanical properties of hot-pressed TiN ceramics with various additives. J Ceram Soc Jpn 1993;101:279–84.
[28] Kenneth H, Laukkanen A, Helena R, Kim W, Simo V. A model for stresses, crack generation and fracture toughness calculation in scratched TiN-coated steel surfaces. Wear 2003;254:278–91.
[29] Guo BG, Zhou JS, Zhang ST, Zhou HD, Pu YP, Chen JM. Phase composition and tribological properties of Ti–Al coatings produced on pure Ti by laser cladding. Appl Surf Sci 2007;253:9301–10.